A. Sap, G. Absillis, T.N. Parac-Vogt, Dalton Transactions 44 (2015) p. 1539-1548
DOI: 10.1039/C4DT01477D

Selective Hydrolysis of Oxidized Insulin Chain B by a Zr(IV)-Substituted Wells-Dawson Polyoxometalate

Annelies Sap,[a] Gregory Absillis,[a] and Tatjana N. Parac-Vogt*[a]

KU Leuven, Department of Chemistry, Celestijnenlaan 200F, B-3001 Heverlee, Belgium.
E-mail: tatjana.vogt@chem.kuleuven.be; Fax: +32 16 327992; Tel: +32 16 327612

We report for the first time on the selective hydrolysis of a polypeptide system by a metal-substituted polyoxometalate (POM). Oxidized insulin chain B, a 30 amino acid polypeptide, was selectively cleaved by the Zr(IV)-substituted Wells-Dawson POM, $K_{15}H[Zr(\alpha_2\text{-}P_2W_{17}O_{61})_2]\cdot 25H_2O$, under physiological pH and temperature conditions in aqueous solution. HPLC-ESI-MS, LC-MS/MS, MALDI-TOF and MALDI-TOF MS/MS data indicate hydrolysis at the Phe1-Val2, Gln4-His5, Leu6-Cys(SO_3H)7, and Gly8-Ser9 peptide bonds. The rate of oxidized insulin chain B hydrolysis (0.45 h^{-1} at pH 7.0 and 60 °C) was calculated by fitting the integration values of its HPLC-UV signal to a first-order exponential decay function. ^{1}H NMR measurements show significant line broadening and shifting of the polypeptide resonances upon addition of the Zr(IV)-POM, indicating that the interaction between the Zr(IV)-POM and the polypeptide takes place in solution. Circular dichroism (CD) measurements clearly prove that the flexible unfolded nature of the polypeptide was retained in the presence of the Zr(IV)-POM. The thermal stability of the Zr(IV)-POM in the presence of the polypeptide chain during the hydrolytic reaction was confirmed by ^{31}P NMR spectroscopy. Despite the highly negative charge of the Zr(IV)-POM, the mechanism of interaction appears to be dominated by a strong metal-directed binding between the positively charged Zr(IV) center and negatively charged amino acid side chains.

Introduction

Despite the importance of structural information to elucidate the functional role of proteins, 3D structure determination of large proteins still remains a big challenge. X-ray crystallography is commonly used to deduce their 3D structure, but it has the limitation that not all proteins can be crystallized. Currently, NMR spectroscopy is widely used to analyze the structure and dynamics of proteins in solution.[1] Another successful approach is controlled hydrolysis of the protein into more manageable fragments that can be traced back to the original protein structure.[2] Therefore, selective hydrolysis of peptides and proteins with different sizes and structures is an important procedure in the fields of bioanalytical chemistry and biotechnology. However, this is a difficult task due to the extreme resistance of the peptide bond towards hydrolysis. In fact, the half-life of the peptide bond is estimated to be between 350-600 years under physiological conditions.[3-5] In order to overcome the extreme stability of the peptide bond, proteolytic enzymes and chemical reagents are often used.

The success of proteolytic enzymes to induce fast cleavage of the peptide bond in proteins can be attributed to their excellent catalytic power. However, several shortcomings limit their use in newly emerging areas of proteomics. Besides the fact that they are expensive, proteolytic enzymes often produce short fragments. Moreover, their self-digestion often leads to contamination of the peptide mixture and more importantly, many of the hydrolytic enzymes also display low sequence specificity.[6,7] These effects seriously complicate the identification process of the native protein. Chemical reagents, such as cyanogen bromide, have been proposed as an alternative to proteolytic enzymes. Unfortunately, protein cleavage often requires harsh reaction conditions which result in denaturation and a loss of structural information. Moreover, they tend to cleave proteins with a limited regioselectivity and only low yields are obtained.[6,7] To circumvent these major drawbacks, different cleaving agents are needed that are able to efficiently induce peptide bond cleavage in a selective manner.

Nowadays, the use of metal-based complexes as artificial peptidases is rising. These transition metal and lanthanide based complexes have proven to be attractive candidates for hydrolyzing the unactivated peptide bond in dipeptides[8-21], oligopeptides[10,14,15,19,22-33], polypeptides[28,34-41] and proteins.[6,12,29,36,42-44] However, metal complexes that efficiently catalyze peptide bond hydrolysis in a regioselective manner under mild reaction conditions still remain scarce.[45] Zr(IV) is often used as the catalytic center and serves as an interesting candidate to promote peptide bond hydrolysis under physiologically relevant conditions of pH and temperature. This is attributed to: (1) its high Lewis acidity, (2) its oxophilic nature, (3) its tendency to form complexes with high coordination numbers and flexible geometries, (4) its kinetic lability, and (5) its redox inactivity.[45]

One major drawback of aqueous solutions of Zr(IV) however, is their strong tendency to form precipitates and insoluble gels upon increasing the pH above 5.0. This can be explained by a polymerization process taking place which induces the formation of Zr(IV) polynuclear polyhydroxo species.[46,47] In an attempt to eliminate precipitation of the Zr(IV) ion and accelerate peptide bond hydrolysis, the azacrown ether 4,13-diazo-18-crown-6 was used as a ligand for complex formation with Zr(IV). Even though this complex enhanced the rate of peptide bond

hydrolysis in neutral solutions, it did not influence the extent of Zr(IV) precipitation.[13,21] As an alternative, polyoxometalates (POMs) can be used to coordinate and stabilize Zr(IV) in aqueous solution.[48]

POMs are generally described as a class of negatively charged metal-oxygen clusters. Their versatile nature with respect to size, shape, polarity, acidity, redox potential, and surface charge distribution makes them attractive chemical agents. In fact, they are applied in various fields such as catalysis, materials science and medicine.[49-52] The biological activity of POMs has been well documented with respect to their antibacterial, antiviral, antiprotozoal, antidiabetic, and anticancer activity.[53-55] Nevertheless, insight in the mechanistic pathways governing this bioactivity at a molecular level remains largely unknown.

To gain more insight into the biological role of POMs, our research group explored the catalytic effect of isopolyoxometalates on a variety of biologically relevant model systems.[56-62] As heteropolyoxotungstates are characterized by a higher stability than isopolyoxometalates, they are considered to be attractive alternative catalysts for a wide range of chemical reactions.[63-69] Indeed, Zr(IV)-substituted POMs have been successfully applied in a range of chemical reactions such as H_2O_2-based oxidations[70-72], the intramolecular cyclization of citronellal[66], the oxidation of sulfides [65,73], Mukaiyama aldol and Mannich-type reactions[74], and phosphoester bond hydrolysis.[75] Recently, our group has demonstrated the peptidase activity of different metal-substituted POMs towards both dipeptides and proteins. For example, Zr(IV)-substituted Wells-Dawson, Keggin, and Lindqvist POMs have shown catalytic activity towards the cleavage of a wide range of dipeptides. They were also able to avoid the formation of inactive Zr(IV) gels, which typically occur at neutral and basic pH values.[76-79] More importantly, a Zr(IV)-substituted Wells-Dawson POM and a Ce(IV)-substituted Keggin POM were shown to selectively hydrolyze albumin proteins and hen-egg-white lysozyme, respectively.[80-82] In this approach, the negatively charged POM ligand interacts with positive protein surface areas, thereby inducing selectivity.[83-91] On the other hand, the Lewis active metal ion serves as the catalytic center and is responsible for the hydrolytic activity of the system.

Studies on peptide bond hydrolysis suggest that the factors influencing the reactivity and selectivity of metal-functionalized POMs towards dipeptides differ from those influencing their reactivity and selectivity towards proteins. In dipeptide systems, the rate of peptide bond hydrolysis is largely influenced by the nature of the amino acid side chain, more specifically its functionality and molecular size.[92,93] However, in larger protein systems, a strong electrostatic component is involved in the binding process. Consequently, the hydrolytic efficiency and site of cleavage are governed by both the size and charge of the POM as well as the protein surface charge distribution.[80] This difference in mechanism of hydrolysis was an incentive to explore the reactivity and selectivity of a metal-substituted POM towards a polypeptide, an intermediate system that has a size in between that of dipeptides and proteins.

In this study, the peptidase activity of a Zr(IV)-substituted Wells-Dawson type POM, $K_{15}H[Zr(\alpha_2\text{-}P_2W_{17}O_{61})_2]\cdot 25H_2O$ (**1**) (Figure 1) towards oxidized insulin chain B was studied in detail. Mass spectrometry methods, NMR spectroscopy, CD spectroscopy and luminescence spectroscopy were used to get insight on the reactivity, selectivity, mechanism of interaction and structural characteristics of both the metal-substituted POM and the polypeptide.

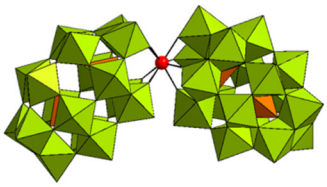

Figure 1: Combined polyhedral/ball-and-stick representation of $K_{15}H[Zr(\alpha_2\text{-}P_2W_{17}O_{61})_2]\cdot 25H_2O$ (**1**). A 1:2 species is displayed in which one Zr(IV) ion coordinates to two Wells-Dawson POM units. The WO_6 octahedrons are displayed in green, the PO_4 tetrahedrons in orange, and the Zr(IV) ion center in red.

Experimental

Chemicals

α-/β-$K_6P_2W_{18}O_{62}\cdot 14/19H_2O$, α_2-$K_{10}P_2W_{17}O_{61}\cdot 20H_2O$, $K_{15}H[Zr(\alpha_2\text{-}P_2W_{17}O_{61})_2]\cdot 25H_2O$ (**1**) and $K_{13}(H_2O)[Eu(H_2O)_{3/4}(\alpha_2\text{-}P_2W_{17}O_{61})_2]\cdot 2\,KCl\cdot n\,H_2O$ (**2**) were synthesized according to the reported procedures[48,94]. Insulin chain B oxidized from bovine pancreas was obtained from Sigma Aldrich and used without any further purification. NaOH was obtained from Fischer scientific and HCl was obtained from AnalaR Normapur. D_2O and NaOD were supplied by Sigma Aldrich. DCl was obtained from Janssen Chimica.

General sample preparation

For the hydrolysis studies, a homogeneous solution of **1** in H_2O (0.5 mM; 1.0 mL) was added to a heterogeneous solution of oxidized insulin chain B in H_2O (0.5 mM, 1.0 mL), resulting in a homogeneous solution of **1** (0.25 mM, 2.0 mL) and oxidized insulin chain B (0.25 mM, 2.0 mL). The solution was thoroughly stirred and the pH of the solution was adjusted to a pH of 7.0 using minor amounts of HCl or NaOH (0.1 M or 0.5 M). The rate constant for the rate of disappearance of the parent peptide, oxidized insulin chain B, was calculated using the rate law for a first-order reaction: $[A]_t = [A]_0 . e^{- kobs.t}$. The half-life was calculated using the formula: $ln(2)/k_{obs}$.

HPLC separations

The components of the reaction mixture were separated by an Agilent 1100 HPLC system equipped with a UV-DAD detector set to 215, 254 and 280 nm. The wavelength range of absorbance for a peptide bond is 190-230 nm.[95] The reversed-phase separations were performed with an analytical Waters X bridge BEH130, C18 column (sized 4.6x250 mm, 3.5 µm beads). In a typical HPLC run, 25 µl of each sample was injected into the system and separations of the reaction mixtures were conducted with a mobile phase gradient elution scheme of 2-98% acetonitrile for 109 min. In all the analytical runs, a flow rate of 0.8 mL/min. was used and the column temperature was maintained at 25 °C. In the HPLC-UV measurements, eluting solvent A was 0.1% (v/v) trifluoroacetic acid in water and solvent B was 0.08% (v/v) trifluoroacetic acid in acetonitrile. In the HPLC-ESI-MS measurements, eluting solvent A was 0.1% (v/v) formic acid in water and solvent B was 100% acetonitrile. All eluents were degassed using an inline vacuum degasser.

Electrospray ionization mass spectrometry

To provide a way of analyzing the content of each reaction mixture, an Agilent 6110 singly-quadrupole ESI-MS was coupled to the Agilent 1100 HPLC system. All the ESI-MS spectra were acquired in positive ion mode. The following ESI instrumental settings were used: Gas Temperature, 350 °C; Drying Gas, 12.0 L/min.; Nebulizer Pressure, 55 psig; Capillary Voltage (positive), 3500 V. The mass spectral peak assignments of the multiply charged peptide fragments were made using the FindPept software. The theoretical isotopic patterns of the peptide fragments were obtained using MS-Isotope tool and compared to the experimental ones.

Tandem mass spectrometry (MS/MS)

The MS/MS measurements were performed on a Thermo Fisher, LCQ Advantage, with an electrospray source and an ion trap analyzer. Data analysis was performed with Xcalibur software of Thermo Fisher. The following ESI source parameters were used: Sheath gas flow = 100 arb, Aux gas flow = 60 arb, Spray voltage = 4.5 kV, Capillary temperature = 270 °C, Capillary voltage = 10 V. All the MS/MS measurements were taken with an isolation width of 2.0 and a 40% collision energy was applied to induce fragmentation. All the MS/MS spectra were taken in positive ion mode.

Matrix-assisted laser desorption mass spectrometry

To prepare the CHCA matrix solution, α-cyano-4-hydroxycinnamic acid (10.0 mg) was first dissolved in 1.0 mL of 1% TFA in H_2O – ACN (30:70, v/v). This solution (22.2 µL) was then pipetted into a 1% TFA in H_2O – ACN (10:90, v/v) solution (200 µL) and the resulting solution was mixed thoroughly. Solutions containing oxidized insulin chain B (0.25 mM) and **1** (0 to 0.5 mM) were diluted 10-fold with 0.1% TFA in H_2O solution. The samples were thoroughly mixed and centrifuged. A total of 1 µL of the sample was transferred on a MALDI sample stage and air-dried. Also, 1 µL of the calibrator was added in between every two spots. Then, 1 µL of the matrix solution was added to each sample and calibrator spot. The MALDI-TOF experiments were performed using a MALDI-TOF Ultraflex II. For all the measurements, α-cyano-4-hydroxycinnamic acid was used as the MALDI matrix and was spotted on the sample to initiate co-crystallization to form the MALDI crystal. A nitrogen laser (337 nm) was then fired at the matrix crystal to induce the ionization process. A laser intensity of 50% with an average of 2000 shots was used. The singly charged peptide fragments were assigned using MASCOT database. The theoretical isotopic patterns of the peptide fragments were obtained using MS-Isotope tool and compared to the experimental ones.

Circular dichroism spectroscopy

Solutions containing oxidized insulin chain B (10.0 µM) and **1** (0 to 20.0 µM) were prepared in H_2O at pH 7.0. CD measurements were performed using a JASCO J-810 spectropolarimeter and each sample was analyzed in a quartz cell with an optical path length of 1 mm. To investigate the secondary structural content of oxidized insulin chain B, all the scans were recorded in the far UV wavelength region (200-260 nm) where peptide bond absorption takes place.[96] For each CD measurement, a baseline correction was performed with the solvent only (100% H_2O) and was subtracted from the actual CD spectrum to account for any background effect.

NMR spectroscopy

For ^{31}P NMR measurements, solutions of **1** (0.5 mM) in the absence and presence of oxidized insulin chain B (0.25 mM) were prepared in D_2O and the pD adjustments were made by adding minor amounts of DCl and NaOD (0.1 M or 0.5 M). The pH-meter reading was corrected by the equation pD = pH + 0.41.[82] For all ^{31}P NMR measurements, 25% H_3PO_4 in D_2O in a sealed capillary tube was used as an external reference. ^{1}H NMR measurements were taken on solutions of oxidized insulin chain B (0.25 mM) in the absence and presence of **1** (0.5 mM) in H_2O and the pH adjustments were made using HCl and NaOH (0.1M or 0.5 M). As an internal reference, TMS was used.

Luminescence spectroscopy

Steady state luminescence spectra were recorded on an Edinburgh Instruments FS900 steady state spectrofluorimeter. Each sample was analyzed in a quartz cell with an optical path length of 10 mm. Spectra of **2** (10^{-4} M) were recorded in H_2O at room temperature at pH 7.0. Excitation of the sample took place at 393 nm and the emission was monitored at 613 nm. Luminescence spectra of **2** were recorded in the absence and presence of polypeptide. The concentrations of polypeptide added were: 1.0 µM, 2.0 µM, 5.0 µM, 10.0 µM, 15.0 µM and 20.0 µM. No higher concentrations of polypeptide could be added due to solubility problems.

Results and discussion

Hydrolysis of oxidized insulin chain B by 1

The hydrolytic reactivity of **1** towards oxidized insulin chain B was examined by mixing equimolar amounts (0.25 mM) of polypeptide and **1** in H_2O (pH 7.0). The reaction mixtures were kept at 37 °C and aliquots were taken at different time intervals. These were then analyzed by HPLC-ESI-MS, LC-MS/MS and MALDI-TOF. A homogeneous reaction mixture was obtained after mixing and neither precipitation nor gel formation was observed during the course of the reaction. The HPLC-ESI-MS spectrum, MALDI-TOF spectrum and MS/MS spectrum of the parent oxidized insulin chain B are displayed in Figure S1, Figure S2 and Figure S3 respectively. An overview of the peptide fragments observed by HPLC-ESI-MS and MALDI-TOF after different incubation times are shown in Table 1 and Table 2 respectively. For all three methods a good agreement was found between the experimental and the theoretical m/z values of both the singly and multiply charged peptide fragments. Therefore these methods can be considered as excellent tools to study the hydrolysis fragments.

A first peptide fragment, Phe1 to Gly8, was formed after approximately 24 h, and was detected by both HPLC-ESI-MS (**Error! Reference source not found.**), and MALDI-TOF (**Error! Reference source not found.**). Moreover, collision induced fragmentation on the peptide fragment, Phe1 to Gly8, was performed by both LC-MS/MS and MALDI-TOF MS/MS. This resulted in a series of product ions, identified as both *N*-terminal b-ions and *C*-terminal y-ions from this peptide fragment (**Error! Reference source not found.**, Figure S7, Table S1). The peaks observed for the doubly charged fragment in the HPLC-ESI-MS spectrum (inset Figure S4) and singly charged fragment in the MALDI-TOF spectrum (Figure S5) display the typical theoretical isotope pattern expected for this fragment. However, the double addition of 0.5 m/z to the doubly charged m/z value of this peptide fragment as well as the double addition of 1.0 m/z to the singly charged m/z value can also be the result of deamidation of Gln4 to Glu4 and/or Asn3 to Asp3. In fact, Zr(IV) ions are known to accelerate hydrolytic deamidation of Gln and Asn residues.[97] The majority of literature reports claim that asparaginyl residues are more susceptible towards hydrolytic deamidation compared to glutamine residues.[98,99] However, our assumption that Gln4 gets deamidated faster than Asn3 is based on the paper of Cepeda et. al[100], where faster deamidation of Gln4 compared to Asn3 occurs in oxidized insulin chain B. In fact, glutamine deamidation has been shown to be accelerated by carboxyl side histidine residues (His5 in oxidized insulin chain B).[100]

After approximately 2 days, a second peptide fragment, identified as Phe1 to Leu6, and a third peptide fragment, with Phe1 to Gln4 as a peptide sequence were detected by HPLC-ESI-MS (Figure S8). LC-MS/MS was also applied on peptide fragment Phe1 to Gln4, resulting in a range of product ions that can be related to the precursor ion. The m/z values of these product ions are shown in **Error! Reference source not found.** and Table S2. It has to be noted, as already mentioned above, that the m/z values of the theoretical isotopic pattern for this fragment are the same as those expected for deamidation of Gln4 to Glu4 and/or Asn3 to Asp3.

At this time interval, HPLC-ESI-MS also detected the terminal amino acid, Phe1, as shown in Figure S10. In both HPLC-ESI-MS and MALDI-TOF, the same peptide fragments and no additional peptide fragments were observed after prolonged incubation times for up to 6 days, suggesting that the cleavage of oxidized insulin chain B by **1** is selective and occurs only at specific sites of the polypeptide.

HPLC-ESI-MS and MALDI-TOF results indicate that hydrolysis of oxidized insulin chain B by **1** results in the following cleavage sites, Gly8-Ser9; Leu6-Cys(SO_3H)7; Gln4-His5; and Phe1-Val2, as shown in Figure 2. A larger number of peptide fragments was observed by HPLC-

ESI-MS compared to MALDI-TOF. In HPLC-ESI-MS, pre-separation of the peptide fragments prior to MS analysis enhances sensitivity. In MALDI-TOF however, complex mixtures with salts can cause competition for charge during the MALDI process, leading to ion suppression.[101]

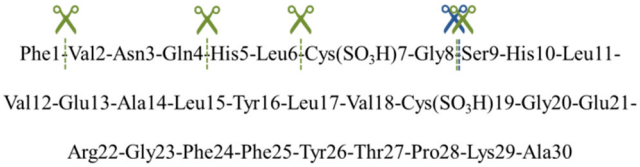

Figure 2: Primary amino acid sequence of oxidized insulin chain B with the corresponding cleavage sites observed at 37 °C and pH 7.0 (green = HPLC-ESI-MS and blue = MALDI-TOF)

To observe the influence of a higher temperature on the selectivity of cleavage, hydrolysis of oxidized insulin chain B by **1** was performed in an equimolar ratio (0.25 mM) at 60 °C at pH 7.0. At this temperature, the same cleavage sites were seen as those observed at 37 °C, with an additional cleavage site observed at Gly20-Glu21 (Figure 3, Table 3). More specifically, the peptide fragment pyroGlu21 to Ala30 with its corresponding isotopic pattern was clearly detected (Figure S11). In fact, metal salts of Zr(IV) are known to accelerate lactimization of *N*-terminal glutamate (Glu) to pyroglutamate (pyroGlu) at 70 °C over a weakly acidic to weakly alkaline pH range.[98] From this experiment it is clear that raising the temperature of the reaction system does not have a major impact on the selectivity of hydrolysis. Moreover, as shown in Table 4, raising the temperature of the hydrolytic reaction to 60 °C resulted in a faster appearance of the peptide fragments in HPLC-ESI-MS and MALDI-TOF.

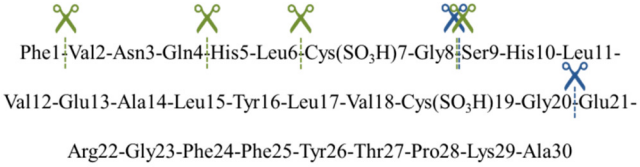

Figure 3: Primary amino acid sequence of oxidized insulin chain B with the corresponding cleavage sites observed at 60 °C and pH 7.0 (green = HPLC-ESI-MS and blue = MALDI-TOF).

Table 1: Overview of multiply charged peptide fragments observed in HPLC-ESI-MS after incubation of equimolar amounts of oxidized insulin chain B and **1** (0.25 mM) at 37 °C and pH 7.0.

Identity of peptide fragment	Letter abbreviation	Charge of peptide fragment	Experimental m/z value	Theoretical m/z value	Peptide bond cleaved	Elution time (min.)
Phe1 to Gly8	C	2+	483.2	483.2	Gly8-Ser9	19.2
Phe1 to Gly8	C	1+	965.3	965.4	Gly8-Ser9	19.2
Phe1 to Leu6	D	2+	379.2	379.2	Leu6-Cys(SO_3H)7	13.4
Phe1 to Leu6	D	1+	757.3	757.4	Leu6-Cys(SO_3H)7	13.4
Phe1 to Gln4	E	1+	507.2	507.2	Gln4-His5	13.4
Phe1 to Gln4	E	2+	254.1	254.1	Gln4-His5	13.4
Phe1	F	1+	166.2	166.1	Phe1-Val2	11.5

Table 2: Peptide fragment observed by MALDI-TOF after incubation of oxidized insulin chain B with **1** in an equimolar ratio (0.25 mM) at 37 °C and pH 7.0.

Identity of peptide fragment	Letter abbreviation	Charge of peptide fragment	Experimental m/z value	Theoretical m/z value	Peptide bond cleaved
Phe1 to Gly8	C	+1	965.4	965.4	Gly8-Ser9

Table 3: Peptide fragments observed by MALDI-TOF after incubation of oxidized insulin chain B with **1** in an equimolar ratio (0.25 mM) at 60 °C and pH 7.0.

Identity of peptide fragment	Letter abbreviation	Charge of peptide fragment	Experimental m/z value	Theoretical m/z value	Peptide bond cleaved
Phe1 to Gly8	C	+1	965.4	965.4	Gly8-Ser9
PyroGlu21 to Ala30	G	+1	1197.5	1197.6	Gly20-Glu21

Table 4: Influence of temperature on the speed of formation of the different peptide fragments obtained by HPLC-ESI-MS/MALDI-TOF for equimolar amounts (0.25 mM) of **1** and oxidized insulin chain B at pH 7.0.

Peptide fragment	T (°C)	Approximate time interval of fragment formation
Phe1 to Gly8	37	24 h
Phe1 to Gly8	60	30 min
Phe1 to Leu6	37	48 h
Phe1 to Leu6	60	8 h
Phe1 to Gln4	37	48 h
Phe1 to Gln4	60	8 h
Phe1	37	48 h
PyroGlu21 to Ala30	60	24 h

Up until now, hydrolysis of oxidized insulin chain B has been studied using a variety of metal salts and/or complexes based on Pd(II), Pt(II), Cu(II), Zn(II), and Zr(IV).[35,37,38,41,102] The resulting peptide fragments were also identified by various mass spectrometry based methods such as ESI-MS, HPLC-ESI-MS, MS/MS and MALDI-TOF. The hydrolytic reactions involving Pd(II)[102], Pt(II)[38], Cu(II)[102], [38] and Zn(II)[37,41] were all conducted under harsh reaction conditions. In fact, strongly acidic pH conditions (pH 2.0 to 2.5) and temperatures ranging from 40 °C to 60 °C were required to induce peptide bond hydrolysis. Interestingly, Cepeda et. al[35] used a Zr(IV) azacrown ether complex to induce hydrolysis of oxidized insulin chain B, at 60 °C and pH 7.0. The fragmentation pattern of oxidized insulin chain B induced by **1** was compared with that promoted by the Zr(IV) azacrown ether complex. This comparison showed that four out of five cleavage sites were seen in both cases: Gly8-Ser9, Leu6-Cys(SO_3H)7, Phe1-Val2 and Gly20-Glu21. However, a total of 13 cleavage sites were reported when the Zr(IV) azacrown ether complex was used, indicating a much less selective hydrolytic cleavage process. This may be related to the fact that a 10-fold molar excess of Zr(IV) was required to hydrolyze oxidized insulin chain B. In addition, the Zr(IV) azacrown ether complex was not able to fully stabilize Zr(IV) as insoluble gels were observed during hydrolysis.[35] The Zr(IV)-complex, **1**, was successful in selectively hydrolyzing oxidized insulin chain B at physiological pH and temperature. Furthermore, no Zr(IV) precipitation was observed, making the Wells-Dawson POM a suitable ligand that stabilizes the Zr(IV) solution.

The disappearance rate of oxidized insulin chain B (0.25 mM) by an excess of **1** (0.5 mM) at pH 7.0 at 60 °C is shown in Figure S12. This graph shows the area of the peak of oxidized insulin chain B seen in HPLC-UV plotted as a function of the time of hydrolysis. Based on this kinetic plot, the rate constant, k_{obs}, of this hydrolytic reaction was calculated to be 0.45 h^{-1} with a corresponding half-life of 1.54 h. This is a significant improvement compared to a previous system in which Zr(IV) was required in a much higher molar excess (500 µM oxidized insulin chain B, 10.0 mM $ZrCl_4$ and 20.0 mM 4,13-diaza-18-crown-6) in order for partial hydrolysis of oxidized insulin chain B to be observed after 4 h.[35] Instead of investigating the disappearance rate of the parent peptide, the appearance rate of the fragments can also be investigated. This was done as an example for the Phe1 to Gly8 fragment. To deduce its rate of formation, the absolute MALDI-TOF intensity cannot be used, as the absolute intensity of the parent peptide varies with each measurement. Instead, the intensity of the peptide fragment was expressed relative to the intensity of the parent peptide at each time interval. This relative intensity increase at physiological pH and temperature is shown in Figure S13 as a function of time. This confirms that the relative amount of this peptide fragment is increasing over time.

Several control experiments were performed to ensure that **1** is responsible for the hydrolysis of oxidized insulin chain B. In a first control experiment, an inhomogeneous solution of oxidized insulin chain B in H_2O was heated at 60 °C at pH 7.0 for up to 6 days in the absence of **1**. Only a negligible amount of peptide fragment Phe1 to Leu6 was observed in HPLC-ESI-MS. In a second control experiment, oxidized insulin chain B was incubated with the α_2-lacunary Wells-Dawson POM, α_2- $K_{10}P_2W_{17}O_{61}\cdot 20H_2O$, in a molar ratio of 1:2 (peptide:lacunary Wells-Dawson POM) in H_2O at 60 °C at pH 7.0 for up to 3 days. No peptide fragments were detected by HPLC-ESI-MS. This proves that the Lewis active Zr(IV) ion is a necessary component contributing to the hydrolytic activity of **1**. In a third control experiment, oxidized insulin chain B

was incubated with $ZrOCl_2.8H_2O$ in a molar ratio of 1:2 (peptide:Zr(IV) salt) in H_2O at 60 °C at pH 5.0 for up to 3 days. This control experiment was carried out at pH 5.0 instead of pH 7.0 because gel formation takes place at neutral pH. A small amount of peptide fragment Phe1 to Gly8 and Phe1 was observed under these conditions. However, insoluble Zr(IV) species were formed resulting in an inhomogeneous solution. Previously, it has been reported that at low pH, Zr(IV) equilibrates as tetranuclear and octanuclear species while hydroxo gels are observed at a higher pH.[46,47] The control experiments therefore suggest that the strongly Lewis acidic Zr(IV) ion contributes to the hydrolytic activity of **1.** They also confirm that the Wells-Dawson POM serves as a stabilizing ligand resulting in a homogeneous reaction mixture at pH 7.0.

Stability and speciation of 1 by ^{31}P NMR spectroscopy

The equilibria between the different Zr(IV) Wells-Dawson species that can exist in solution are displayed in Figure 4.[103-105] The type of Zr(IV) Wells-Dawson species present in solution depends on various factors such as concentration, temperature, pH, and time.[76] ^{31}P NMR measurements were performed on **1** (0.5 mM) in the absence and presence of oxidized insulin chain B (0.25 mM) in D_2O at pD 7.0 at 60 °C. In the ^{31}P NMR spectrum of pure **1**, only 2 peaks were observed at -9.29 ppm and -13.90 ppm. The chemical shift difference between the two peaks is 4.61 ppm, which typically corresponds to the 1:2 species.[48] This was expected, as it was previously demonstrated that the 1:2 species is favored under this pH condition.[76] Upon addition of oxidized insulin chain B, no changes in the ^{31}P NMR spectrum were observed. Only the 1:2 species was observed, implying that this is the active species inducing peptide bond hydrolysis. Moreover, this species was maintained after heating the solution at 60 °C for 6 days. This proves the thermal stability of **1** throughout the hydrolytic reaction (Figure S14). The x-ray crystal structure of the 1:2 species however does not show any free coordination sites for binding to oxidized insulin chain B. It is plausible that decoordination of one POM ligand takes place in solution leading to free coordination sites on Zr(IV) that can coordinate and activate the polypeptide towards hydrolysis. This process is too fast to be detected by ^{31}P NMR. Theoretical studies are currently being carried out in our group in order to get a better understanding on this process.

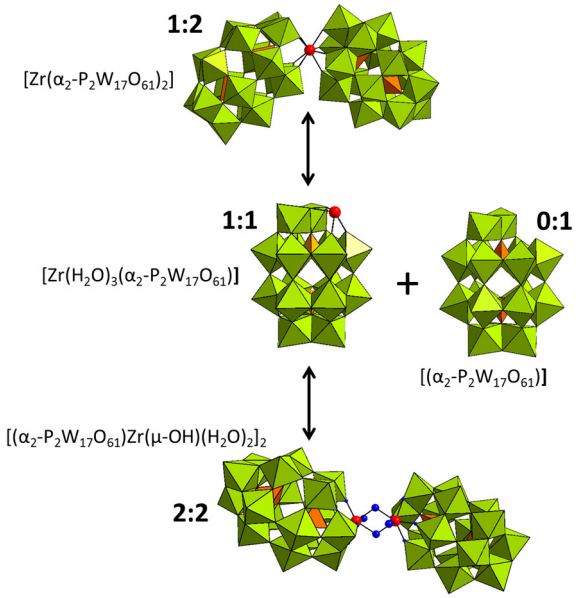

Figure 4: Equilibria between the different Zr(IV)-substituted Wells-Dawson type species in aqueous solution: 1:2 dimeric species $[Zr(\alpha_2\text{-}P_2W_{17}O_{61})_2]$, 1:1 monosubstituted species $[Zr(H_2O)_3(\alpha_2\text{-}P_2W_{17}O_{61})]$ and 2:2 dimeric species with two hydroxo bridges in the middle $[(\alpha_2\text{-}P_2W_{17}O_{61})Zr(\mu\text{-}OH)(H_2O)_2]_2$.

Interaction between oxidized insulin chain B and 1

^{1}H NMR spectra of oxidized insulin chain B (0.25 mM) in the absence and presence of **1** (0.5 mM) were taken at pH 7.0 in H_2O. Upon addition of **1**, line-broadening and clear changes in the chemical shift in the aliphatic, aromatic and N-H region were observed (Figure S15 and Figure S16). By adding **1** to oxidized insulin chain B potassium ions are introduced in the mixture. While an increase in ionic strength can result in changes in the environment of the polypeptide leading to chemical shift changes, line-broadening is typically the result of an interaction process. Therefore the combined line-broadening and chemical shift changes are ascribed to interaction between **1** and oxidized insulin chain B.

Eu(III) luminescence spectroscopy has been proven as a useful tool to study interactions between Eu(III)-based POMs and proteins.[83,84,89,91] The mechanism of interaction has usually been explained by a substitution of water molecules, bound to the Eu(III) ion, by the protein. This results in an increase of Eu(III) luminescence intensity and in a rise of the luminescence lifetime of the Eu(III) ion.[91] In contrary, addition of glycine-based oligopeptides (with 3 to 5 amino acids) to **1** did not result in the change of relative intensity of Eu(III) luminescence. This

suggests that a defined tertiary structure and charge distributions, which are present in proteins, leads to specific electrostatic interaction with the highly negatively charged surface of the POM. To gain insight into the interaction behavior between **1** and oxidized insulin chain B, the luminescence of a Eu(III) Wells-Dawson POM (Figure S18)[94,106], which is structurally analogous to **1** but hydrolytically inactive, was investigated in the absence and presence of the polypeptide. Similarly to short peptides, no major changes in the relative intensity of Eu(III) were observed in the emission spectrum of Eu(III) Wells-Dawson POM upon the addition of increasing concentrations of oxidized insulin chain B. This is not surprising however, as oxidized insulin chain B is a flexible 30-mer polypeptide with a low net charge of -2 at pH 7. The interaction of oxidized insulin chain B with the Zr(IV) Wells-Dawson POM therefore appears to be primarily based on coordination with the metal ion rather than with the negative POM surface, as observed in the case of proteins.

To gain insight into the structural content of oxidized insulin chain B in the absence and presence of **1**, CD spectroscopic measurements were further performed. The addition of a POM to a protein can either stabilize or destabilize the protein or not alter the secondary structure of the protein at all.[83,86-88,107] We have previously shown that binding of a Ce(IV) Keggin POM to HEWL resulted in a decrease in the degree of alpha helicity of the protein.[80] To understand the effect of POM addition on the secondary structure of oxidized insulin chain B, the far UV region of the CD spectrum (190-250 nm), where peptide bond absorption takes place, was screened. In the CD spectrum of pure oxidized insulin chain B at room temperature at pH 7.0 in aqueous solution, a large minimum was observed at approximately 200 nm. This feature is indicative of a completely random coil conformation, which has also been reported in literature at pH 3.6.[108] This random coil conformation was retained upon addition of up to 20.0 μM of **1**, as shown in Figure S17. It can therefore be concluded that addition of **1** did not induce any change in the flexible nature of oxidized insulin chain B.

Proposed reaction pathways

The combination of different mass spectrometry techniques has unambiguously indicated that oxidized insulin chain B has been selectively cleaved at the Phe1-Val2, Gln4-His5, Leu6-Cys(SO_3H)7 Gly8-Ser9 peptide bonds at physiological pH and temperature. The first cleavage site to be hydrolyzed in oxidized insulin chain B by **1** was the Gly8-Ser9 peptide bond, which has also been identified as a cleavage site in the presence of other metal complexes.[35,38,41,102] Moreover, it has been previously shown to have a very high susceptibility towards hydrolysis by metal-substituted POMs in dipeptides.[78,92] However, this peptide bond does not appear to be hydrolyzed by metal-substituted POMs in proteins that were previously studied.[80,81] The high reactivity of the Gly-Ser bond in dipeptides and polypeptides is explained by the hydroxyl group of serine promoting a N => O acyl rearrangement. This eventually leads to hydrolysis of the Gly8-Ser9 bond.[57,78,109] The second cleavage site, between residues Leu6 and Cys(SO_3H)7, has also been hydrolyzed by a Pd(II) and Zr(IV) azacrown ether complex.[35,102] The most likely mechanism involves the initial anchoring of the Zr(IV) center to the imidazole N in His5, which is known to be a suitable binding site for metal ions.[77,102] The negatively charged sulfonate group could act as a ligand for the positively charged Zr(IV) center inducing an additional electrostatic interaction. This interaction can direct Zr(IV) that is anchored to the imidazole N of His5 closer to the carbonyl group of Leu6, causing its polarization and accelerating the cleavage of the Leu6-Cys(SO_3H)7 bond.[102] For the third cleavage site, Gln4-His5, the N in the imidazole ring of His5 can again serve as a potential binding site, leading to cleavage of this peptide bond. Additionally, deamidation to Glu4 can induce an electrostatic interaction between the positively charged Zr(IV) with the negatively charged carboxylate side chain in Glu4, leading to hydrolysis of Gln4-His5. To the best of our knowledge, this peptide bond has not been hydrolyzed by other transition metal complexes reported in the literature. For the fourth cleavage site, Phe1-Val2, peptide bond hydrolysis by **1** could be easily induced by the coordination of the Zr(IV) center to the N-terminal amino group of Phe1. The cleavage of this peptide bond has also been promoted by other metal complexes.[35,37,38] An additional cleavage site, Gly20-Glu21, has been observed in oxidized insulin chain B upon an increase in temperature. This peptide bond has also been hydrolyzed by the Zr(IV) azacrown ether complex.[35] The hydrolysis site could be promoted by an electrostatic interaction between the negatively charged carboxylate group in the side chain of glutamic acid and the positively charged Zr(IV) center. Negatively charged amino acids, such as cysteine sulfonic acid and glutamic acid, are often found in the vicinity of the hydrolyzed peptide bond. These amino acids serve as important residues for electrostatic interaction with the positively charged Zr(IV) center. However, no peptide bond is hydrolyzed in the vicinity of Glu13, which may be a result of the steric hindrance of the neighboring Val12 and Ala14.

In summary, the selectivity of hydrolysis of a large polypeptide with no defined secondary structural elements closely resembles the selectivity observed in dipeptides. This selectivity seems to be dominated by coordination of the positively charged Zr(IV) ion to the amino acid residue rather than by the electrostatic interaction with the negatively charged POM ligand. This hydrolysis mechanism may be attributed to the small, flexible nature of the polypeptide chain. In contrast, larger proteins have a defined tertiary structure and charge distribution that contribute to additional electrostatic interaction with the negatively charged Wells-Dawson POM ligand. This in turn results in the regioselective hydrolysis of the protein.[81] We therefore believe that increasing the positive charge of the polypeptide chain will only result in electrostatic interaction with the negatively charged POM surface when these positive charges are grouped due to folding in a surface patch to which the POM ligand can dock.

Conclusions

This study offers further insight into the factors influencing the reactivity and selectivity of metal-functionalized POMs towards polypeptide systems. Previous studies on short peptides have shown that the selectivity of peptide bond hydrolysis is largely influenced by the nature of the amino acid side chain, while in larger protein systems, a strong electrostatic component also influences the selectivity. In this work, the reactivity and selectivity of a metal-substituted POM towards a large polypeptide, oxidized insulin chain B, a flexible 30-mer polypeptide which is an intermediate system between dipeptides and proteins, has been examined. Hydrolysis of the polypeptide has been achieved under physiological pH and temperature in a fast and selective manner. Up until now, cleavage of oxidized insulin chain B either required relatively high temperatures and acidic pH conditions or resulted in a non-selective cleavage pattern. In the present study, we have successfully addressed this limitation. The selectivity of hydrolysis was driven by coordination chemistry between the Zr(IV) ion in the POM and the polypeptide, while no evidence of the specific electrostatic interactions was observed. The flexible nature of the polypeptide chain with its specific type and order of amino acid residues is responsible for the observed selectivity of cleavage driven by **1**. In the future, this understanding may facilitate structural studies of similar polypeptides and advance the application of metal-substituted POMs as a novel class of artificial metalloproteases.

Acknowledgements

T.N.P.V. thanks KU Leuven research fund and FWO Flanders (Belgium) for financial support. A.S. thanks the FWO Flanders (Belgium) for a doctoral fellowship. G.A. thanks the FWO Flanders for a post-doctoral fellowship. We thank Prof. J.P. Noben and Mr. E. Royackers for their advice on the use of MALDI-TOF equipment.

Notes and references

[a]KU Leuven, Department of Chemistry, Celestijnenlaan 200F, B-3001 Heverlee, Belgium. Fax: +32 16 327992; Tel: +32 16 327612; Email: tatjana.vogt@chem.kuleuven.be.

† Electronic Supplementary Information (ESI) available: HPLC-ESI-MS spectra, MALDI-TOF spectra and MS/MS spectra of the peptide fragments. Kinetic data, CD spectroscopy data and NMR spectroscopy data are provided. See DOI: 10.1039/b000000x/

1 K. Wüthrich, *Nature Structural and Molecular Biology*, 2001, **8**, 923-925.
2 R. Westermeier and T. Naven, *Proteomics in Practice: A Laboratory Manual of Proteome Analysis*, Wiley-VCH Verlag-GmbH, Weinheim, 2002.
3 A. Radzicka and R. Wolfenden, *Journal of the American Chemical Society*, 1996, **118**, 6105-6109.
4 R. M. Smith and D. E. Hansen, *Journal of the American Chemical Society*, 1998, **120**, 8910-8913.
5 R. A. R. Bryant and D. E. Hansen, *Journal of the American Chemical Society*, 1996, **118**, 5498-5499.
6 L. Zhu, R. Bakhtiar and N. M. Kostic, *Journal of Biological Inorganic Chemistry*, 1998, **3**, 383-391.
7 E. N. Korneeva, M. V. Ovchinnikov and N. M. Kostic, *Inorganica Chimica Acta*, 1996, **243**, 9-13.
8 N. V. Kaminskaia and N. M. Kostic, *Inorganic Chemistry*, 2001, **40**, 2368-2377.
9 S. U. Milinkovic, T. N. Parac, M. I. Djuran and N. M. Kostic, *Journal of the Chemical Society-Dalton Transactions*, 1997, 2771-2776.
10 L. G. Zhu and N. M. Kostic, *Inorganica Chimica Acta*, 1994, **217**, 21-28.
11 M. Yashiro, T. Takarada, S. Miyama and M. Komiyama, *Journal of the Chemical Society-Chemical Communications*, 1994, 1757-1758.
12 E. L. Hegg and J. N. Burstyn, *Journal of the American Chemical Society*, 1995, **117**, 7015-7016.
13 M. Kassai and K. B. Grant, *Inorganic Chemistry Communications*, 2008, **11**, 521-525.
14 S. Manka, F. Becker, O. Hohage and W. S. Sheldrick, *Journal of Inorganic Biochemistry*, 2004, **98**, 1947-1956.
15 A. Erxleben, *Inorganic Chemistry*, 2005, **44**, 1082-1094.
16 T. N. Parac, G. M. Ullmann and N. M. Kostic, *Journal of the American Chemical Society*, 1999, **121**, 3127-3135.
17 T. N. Parac and N. M. Kostic, *Journal of the American Chemical Society*, 1996, **118**, 51-58.
18 G. B. Karet and N. M. Kostic, *Inorganic Chemistry*, 1998, **37**, 1021-1027.
19 I. E. Burgeson and N. M. Kostic, *Inorganic Chemistry*, 1991, **30**, 4299-4305.
20 T. W. Johnson and N. M. Kostic, *Journal of the Serbian Chemical Society*, 2004, **69**, 887-899.
21 M. Kassai, R. G. Ravi, S. J. Shealy and K. B. Grant, *Inorganic Chemistry*, 2004, **43**, 6130-6132.
22 S. Rajkovic, B. D. Glisic, M. D. Zivkovic and M. I. Djuran, *Bioorganic Chemistry*, 2009, **37**, 173-179.
23 J. Hong, Y. Jiao, W. He, Z. Guo, Z. Yu, J. Zhang and L. Zhu, *Inorganic Chemistry*, 2010, **49**, 8148-8154.
24 M. I. Djuran and S. U. Milinkovic, *Polyhedron*, 1999, **18**, 3611-3616.
25 N. M. Milovic and N. M. Kostic, *Journal of the American Chemical Society*, 2003, **125**, 781-788.
26 T. Takarada, M. Yashiro and M. Komiyama, *Chemistry-a European Journal*, 2000, **6**, 3906-3913.
27 E. Kopera, A. Krezel, A. M. Protas, A. Belczyk, A. Bonna, A. Wyslouch-Cieszynska, J. Poznanski and W. Bal, *Inorganic Chemistry*, 2010, **49**, 6636-6645.
28 N. M. Milovic and N. M. Kostic, *Journal of the American Chemical Society*, 2002, **124**, 4759-4769.
29 L. M. Dutca, K. S. Ko, N. L. Pohl and N. M. Kostic, *Inorganic Chemistry*, 2005, **44**, 5141-5146.
30 A. M. Protas, A. Bonna, E. Kopera and W. Bal, *Journal of Inorganic Biochemistry*, 2011, **105**, 10-16.
31 A. Krezel, M. Mylonas, E. Kopera and W. Bal, *Acta Biochimica Polonica*, 2006, **53**, 721-727.
32 A. Kumar, X. Zhu, K. Walsh and R. Prabhakar, *Inorganic Chemistry*, 2010, **49**, 38-46.
33 V. Yeguas, P. Campomanes, R. Lopez, N. Diaz and D. Suarez, *Journal of Physical Chemistry B*, 2010, **114**, 8525-8535.
34 T. N. Parac and N. M. Kostic, *Inorganic Chemistry*, 1998, **37**, 2141-2144.
35 S. S. Cepeda and K. B. Grant, *New Journal of Chemistry*, 2008, **32**, 388-391.

36 N. M. Milovic, L. M. Dutca and N. M. Kostic, *Inorganic Chemistry*, 2003, **42**, 4036-4045.
37 J. Jiang, Q. J. Wu, X. Y. Cai, L. G. Zhu and W. J. Wang, *Chinese Chemical Letters*, 2009, **20**, 71-75.
38 J. Hong, R. Miao, C. Zhao, J. Jiang, H. Tang, Z. Guo and L. Zhu, *Journal of Mass Spectrometry*, 2006, **41**, 1061-1072.
39 Y. P. Ho, H. P. Li and L. C. Lu, *International Journal of Mass Spectrometry*, 2003, **227**, 97-109.
40 A. Krezel, E. Kopera, A. M. Protas, J. Poznanski, A. Wyslouch-Cieszynska and W. Bal, *Journal of the American Chemical Society*, 2010, **132**, 3355-3366.
41 J. Jiang, Y. H. Mei, L. G. Zhu and W. J. Wang, *Chinese Chemical Letters*, 2007, **18**, 557-560.
42 L. G. Zhu, L. Qin, T. N. Parac and N. M. Kostic, *Journal of the American Chemical Society*, 1994, **116**, 5218-5224.
43 L. Zhu and N. M. Kostic, *Inorganica Chimica Acta*, 2002, **339**, 104-110.
44 N. M. Milovic, L. M. Dutca and N. M. Kostic, *Chemistry-a European Journal*, 2003, **9**, 5097-5106.
45 K. B. Grant and M. Kassai, *Current Organic Chemistry*, 2006, **10**, 1035-1049.
46 A. Singhal, L. M. Toth, J. S. Lin and K. Affholter, *Journal of the American Chemical Society*, 1996, **118**, 11529-11534.
47 A. Clearfield, *Journal of Materials Research*, 1990, **5**, 161-162.
48 C. N. Kato, A. Shinohara, K. Hayashi and K. Nomiya, *Inorganic Chemistry*, 2006, **45**, 8108-8119.
49 A. Proust, R. Thouvenot and P. Gouzerh, *Chemical Communications*, 2008, 1837-1852.
50 J. T. Rhule, C. L. Hill and D. A. Judd, *Chemical Reviews*, 1998, **98**, 327-357.
51 D.-L. Long, R. Tsunashima and L. Cronin, *Angewandte Chemie-International Edition*, 2010, **49**, 1736-1758.
52 D.-L. Long, E. Burkholder and L. Cronin, *Chemical Society Reviews*, 2007, **36**, 105-121.
53 A. Fluetsch, T. Schroeder, M. G. Gruetter and G. R. Patzke, *Bioorganic & Medicinal Chemistry Letters*, 2011, **21**, 1162-1166.
54 H. Yanagie, A. Ogata, S. Mitsui, T. Hisa, T. Yamase and M. Eriguchi, *Biomedicine & Pharmacotherapy*, 2006, **60**, 349-352.
55 A. Ogata, S. Mitsui, H. Yanagie, H. Kasano, T. Hisa, T. Yamase and M. Eriguchi, *Biomedicine & Pharmacotherapy*, 2005, **59**, 240-244.
56 G. Absillis, E. Cartuyvels, R. Van Deun and T. N. Parac-Vogt, *Journal of the American Chemical Society*, 2008, **130**, 17400-17408.
57 H. Phuong Hien, K. Stroobants and T. N. Parac-Vogt, *Inorganic Chemistry*, 2011, **50**, 12025-12033.
58 P. H. Ho, E. Breynaert, C. E. A. Kirschhock and T. N. Parac-Vogt, *Dalton Transactions*, 2011, **40**, 295-300.
59 N. Steens, A. M. Ramadan, G. Absillis and T. N. Parac-Vogt, *Dalton Transactions*, 2010, **39**, 585-592.
60 N. Steens, A. M. Ramadan and T. N. Parac-Vogt, *Chemical Communications*, 2009, 965-967.
61 L. Van Lokeren, E. Cartuyvels, G. Absillis, R. Willem and T. N. Parac-Vogt, *Chemical Communications*, 2008, 2774-2776.
62 E. Cartuyvels, G. Absillis and T. N. Parac-Vogt, *Chemical Communications*, 2008, 85-87.
63 N. Mizuno, K. Yamaguchi and K. Kamata, *Coordination Chemistry Reviews*, 2005, **249**, 1944-1956.
64 N. Mizuno, K. Kamata and K. Yamaguchi, *Topics in Catalysis*, 2010, **53**, 876-893.
65 M. Carraro, N. Nsouli, H. Oelrich, A. Sartorel, A. Soraru, S. S. Mal, G. Scorrano, L. Walder, U. Kortz and M. Bonchio, *Chemistry-a European Journal*, 2011, **17**, 8371-8378.
66 Y. Kikukawa, S. Yamaguchi, Y. Nakagawa, K. Uehara, S. Uchida, K. Yamaguchi and N. Mizuno, *Journal of the American Chemical Society*, 2008, **130**, 15872-15878.
67 M. Orlandi, R. Argazzi, A. Sartorel, M. Carraro, G. Scorrano, M. Bonchio and F. Scandola, *Chemical Communications*, 2010, **46**, 3152-3154.
68 V. Torsvik, L. Ovreas and T. F. Thingstad, *Science*, 2002, **296**, 1064-1066.
69 C. Boglio, B. Hasenknopf, G. Lenoble, P. Remy, P. Gouzerh, S. Thorimbert, E. Lacote, M. Malacria and R. Thouvenot, *Chemistry-a European Journal*, 2008, **14**, 1532-1540.
70 O. A. Kholdeeva, G. M. Maksimov, R. I. Maksimovskaya, M. P. Vanina, T. A. Trubitsina, D. Y. Naumov, B. A. Kolesov, N. S. Antonova, J. J. Carbo and J. M. Poblet, *Inorganic Chemistry*, 2006, **45**, 7224-7234.
71 O. A. Kholdeeva and R. I. Maksimovskaya, *Journal of Molecular Catalysis a-Chemical*, 2007, **262**, 7-24.
72 G. Al-Kadamany, S. S. Mal, B. Milev, B. G. Donoeva, R. I. Maksimovskaya, O. A. Kholdeeva and U. Kortz, *Chemistry-a European Journal*, 2010, **16**, 11797-11800.
73 C. Jahier, S. S. Mal, U. Kortz and S. Nlate, *European Journal of Inorganic Chemistry*, 2010, 1559-1566.
74 N. Dupre, P. Remy, K. Micoine, C. Boglio, S. Thorimbert, E. Lacote, B. Hasenknopf and M. Malacria, *Chemistry-a European Journal*, 2010, **16**, 7256-7264.
75 S. Vanhaecht, G. Absillis and T. N. Parac-Vogt, *Dalton Transactions*, 2012, **41**, 10028-10034.
76 G. Absillis and T. N. Parac-Vogt, *Inorganic Chemistry*, 2012, **51**, 9902-9910.
77 H. G. T. Ly, G. Absillis, S. R. Bajpe, J. A. Martens and T. N. Parac-Vogt, *European Journal of Inorganic Chemistry*, 2013, **2013**, 4601-4611.
78 H. G. T. Ly, G. Absillis and T. N. Parac-Vogt, *Dalton Transactions*, 2013, **42**, 10929-10938.
79 K. Takeda, M. Shigeta and K. Aoki, *Journal of Colloid and Interface Science*, 1987, **117**, 120-126.
80 K. Stroobants, E. Moelants, H. G. T. Ly, P. Proost, K. Bartik and T. N. Parac-Vogt, *Chemistry-a European Journal*, 2013, **19**, 2848-2858.
81 K. Stroobants, G. Absillis, E. Moelants, P. Proost and T. Parac-Vogt, *Chemistry-a European Journal*, 2014, **20**, 3894-3897.
82 K. Stroobants, V. Goovaerts, G. Absillis, E. Moelants, P. Proost and T. N. Parac-Vogt, *Chemistry-a European Journal*, DOI: 10.1002/chem.201402683.
83 Z. Li, M. Ying, Z. Guangjin, Y. Jiannian, B. Keita and L. Nadjo, *Physical Chemistry Chemical Physics*, 2010, **12**, 1299-1304.
84 G. Hungerford, K. Suhling and M. Green, *Photochemical & Photobiological Sciences*, 2008, **7**, 734-737.
85 L. Zheng, Z. Gu, Y. Ma, G. Zhang, J. Yao, B. Keita and L. Nadjo, *Journal of Biological Inorganic Chemistry*, 2010, **15**, 1079-1085.
86 L. Zheng, Y. Ma, G. Zhang, J. Yao, B. S. Bassil, U. Kortz, B. Keita, P. de Oliveira, L. Nadjo, C. T. Craescu and S. Miron, *European Journal of Inorganic Chemistry*, 2009, 5189-5193.
87 G. Zhang, B. Keita, C. T. Craescu, S. Miron, P. de Oliveira and L. Nadjo, *Biomacromolecules*, 2008, **9**, 812-817.
88 Z. Guangjin, B. Keita, C. T. Craescu, S. Miron, P. de Oliveira and L. Nadjo, *Journal of Physical Chemistry B*, 2007, **111**, 11253-11259.
89 G. Hungerford, F. Hussain, G. R. Patzke and M. Green, *Physical Chemistry Chemical Physics*, 2010, **12**, 7266-7275.
90 H. Stephan, M. Kubeil, F. Emmerling and C. E. Mueller, *European Journal of Inorganic Chemistry*, 2013, 1585-1594.
91 V. Goovaerts, K. Stroobants, G. Absillis and T. N. Parac-Vogt, *Physical Chemistry Chemical Physics*, 2013, **15**, 18378-18387.
92 S. Vanhaecht, G. Absillis and T. N. Parac-Vogt, *Dalton Transactions*, 2013, **42**, 15437-15446.
93 H. Czapor-Irzabek, M. Cebrat, Z. Czyznikowska and J. Brasun, *Journal of Inorganic Biochemistry*, 2012, **110**, 40-45.
94 C. Zhang, L. Bensaid, D. McGregor, X. Fang, R. C. Howell, B. Burton-Pye, Q. Luo, L. Todaro and L. C. Francesconi, *Journal of Cluster Science*, 2006, **17**, 389-425.
95 A. R. Goldfarb, L. J. Saidel and E. Mosovich, *J. Biol. Chem.*, 1951, **193**, 397-404.
96 S. M. Kelly and N. C. Price, *Current Protein & Peptide Science*, 2000, **1**, 349-384.

97 E. Bamann, H. Trapmann and H. Muenstermann, *Arch. Pharm.*, 1963, **296**, 47-53.
98 E. Bamann and Munsterm.H, *Archiv Der Pharmazie Und Berichte Der Deutschen Pharmazeutischen Gesselschaft*, 1965, **298**, 750-&.
99 A. B. Robinson and C. J. Rudd, *Curr. Top. Cell. Regul.*, 1974, **8**, 247-295.
100 S. S. Cepeda, *Chemistry dissertations*, 2009.
101 V. C. Chen, K. Cheng, W. Ens, K. G. Standing, J. I. Nagy and H. Perreault, *Analytical Chemistry*, 2004, **76**, 1189-1196.
102 X. M. Luo, W. J. He, Y. Zhang, Z. J. Guo and L. G. Zhu, *Chinese Journal of Chemistry*, 2000, **18**, 855-862.
103 Y. Saku, Y. Sakai and K. Nomiya, *Inorganica Chimica Acta*, 2010, **363**, 967-974.
104 M. N. Sokolov, N. V. Izarova, E. V. Peresypkina, A. V. Virovets and V. P. Fedin, *Russian Chemical Bulletin*, 2009, **58**, 507-512.
105 M. N. Sokolov, N. V. Izarova, E. V. Peresypkina, D. A. Mainichev and V. P. Fedin, *Inorganica Chimica Acta*, 2009, **362**, 3756-3762.
106 Q. H. Luo, R. C. Howell, M. Dankova, J. Bartis, C. W. Williams, W. D. Horrocks, V. G. Young, A. L. Rheingold, L. C. Francesconi and M. R. Antonio, *Inorganic Chemistry*, 2001, **40**, 1894-1901.
107 G. Zhang, B. Keita, J.-C. Brochon, P. de Oliveira, L. Nadjo, C. T. Craescu and S. Miron, *Journal of Physical Chemistry B*, 2007, **111**, 1809-1814.
108 F. Y. Dupradeau, T. Richard, G. Le Flem, H. Oulyadi, Y. Prigent and J. P. Monti, *Journal of Peptide Research*, 2002, **60**, 56-64.
109 M. Yashiro, Y. Sonobe, A. Yamamura, T. Takarada, M. Komiyama and Y. Fujii, *Organic & Biomolecular Chemistry*, 2003, **1**, 629-632.

Supplementary information

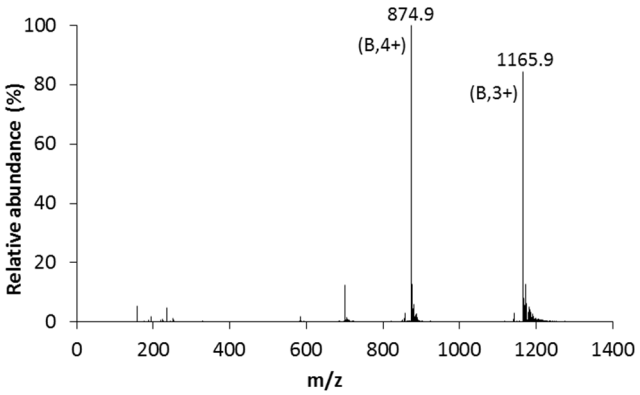

Figure S1: HPLC-ESI-MS spectrum of oxidized insulin chain B (full parent peptide B) with an HPLC elution time of 47.4 min. Both the triply (1165.9) and quarterly (874.9) charged mass of the parent peptide are shown.

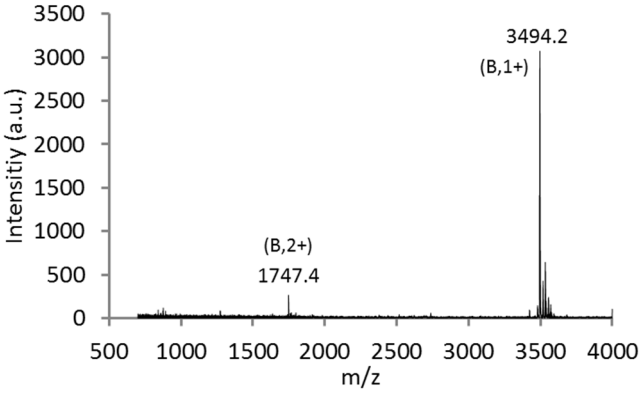

Figure S2: MALDI-TOF spectrum of oxidized insulin chain B (full parent peptide B) showing both the singly charged (3494.2) and doubly (1747.4) charged mass of the parent peptide.

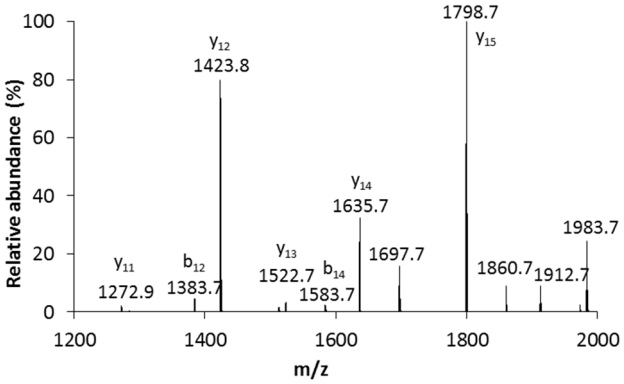

Figure S3: LC-MS/MS spectrum of oxidized insulin chain B. Both *N*-terminal b-ions and *C*-terminal y-ions are shown.

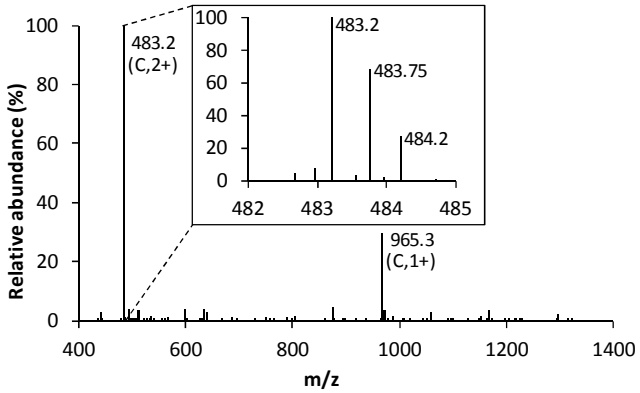

Figure S4: HPLC-ESI-MS spectrum of peptide fragment C, *Phe1 to Gly8*, with an HPLC elution time of 19.2 min. Both the doubly charged (483.2) and singly charged (965.3) mass corresponding to this hydrolysis fragment are shown. The corresponding isotopic pattern of the doubly charged fragment is shown as an inset.

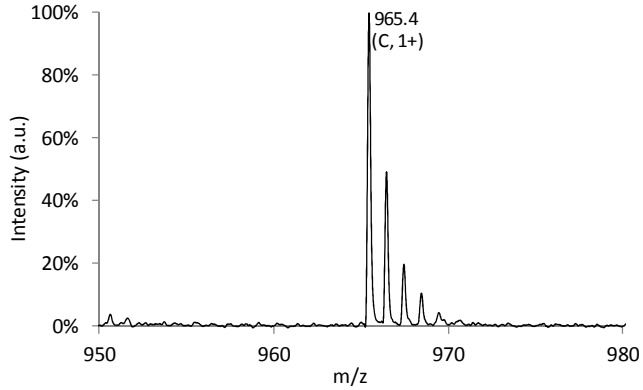

Figure S5: MALDI-TOF spectrum of singly charged peptide fragment C, *Phe1 to Gly8* (965.4) with its corresponding isotopic pattern.

A. Sap, G. Absillis, T.N. Parac-Vogt, Dalton Transactions 44 (2015) p. 1539-1548
DOI: 10.1039/C4DT01477D

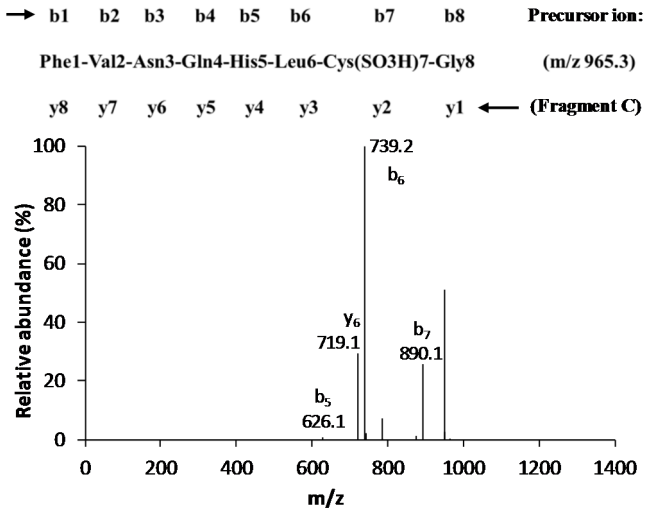

Figure S6: LC-MS/MS spectrum generated from the peptide fragment *Phe1 to Gly8*. Both *N*-terminal b-ions and *C*-terminal y-ions are shown.

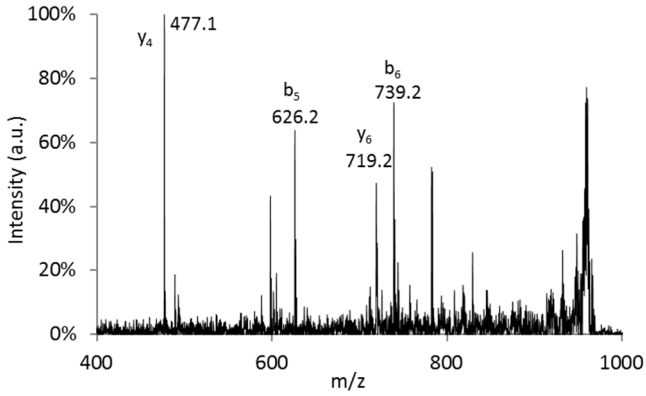

Figure S7: MALDI-TOF MS/MS generated from the peptide fragment *Phe1 to Gly8*. Both *N*-terminal b-ions and *C*-terminal y-ions are shown.

Table S1: MS/MS data from LC-MS/MS and MALDI-TOF MS/MS of the peptide fragment, *Phe1 to Gly8*, showing both the *N*-terminal b-ions and *C*-terminal y-ions.

Experimental m/z value	Theoretical m/z value	Peptide fragment	Charge	Type of ion
477.1	477.2	His5 to Gly8	1+	y_4 ion
626.2	626.3	Phe1 to His5	1+	b_5 ion
719.2	719.3	Asn3 to Gly8	1+	y_6 ion
739.2	739.4	Phe1 to Leu6	1+	b_6 ion
890.1	890.4	Phe1 to Cys(SO_3H)7	1+	b_7 ion
947.1	947.4	Phe1 to Gly8	1+	b_8 ion

A. Sap, G. Absillis, T.N. Parac-Vogt, Dalton Transactions 44 (2015) p. 1539-1548
DOI: 10.1039/C4DT01477D

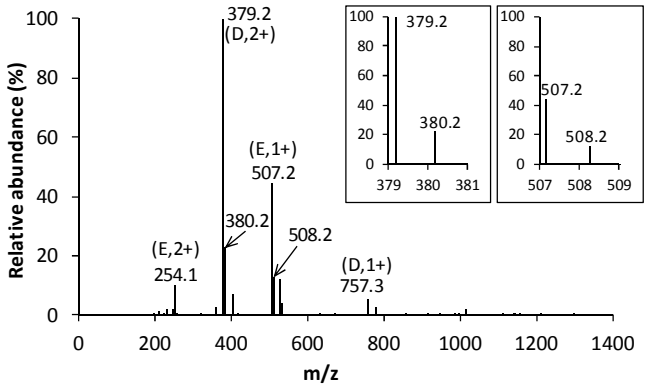

Figure S8: HPLC-ESI-MS spectrum of peptide fragments D and E, *Phe1 to Leu6* and *Phe1 to Gln4 respectively*, with an HPLC elution time of 13.4 min. Both the doubly charged (379.2) and singly charged (757.3) mass corresponding to hydrolysis fragment *Phe1 to Leu6* are shown. Both the singly charged (507.2) and doubly charged (254.1) mass corresponding to hydrolysis fragment *Phe1 to Gln4* are shown.

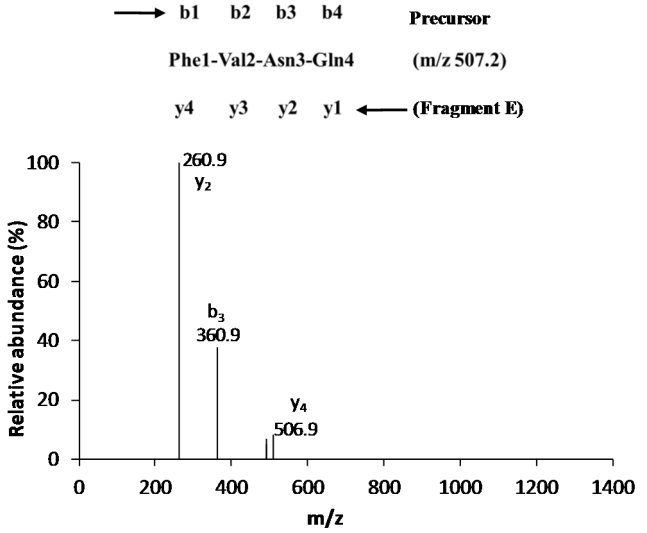

Figure S9: LC-MS/MS spectrum generated from the peptide fragment *Phe1 to Gln4*. Both *N*-terminal b-ions and *C*-terminal y-ions are shown.

Table S2: MS/MS data of the peptide fragment, *Phe1 to Gln4*, showing both the *N*-terminal b-ions and *C*-terminal y-ions.

Experimental m/z value	Theoretical m/z value	Peptide fragment	Charge	Type of ion
260.9	261.1	Asn3 to Gln4	1+	y_2 ion
360.9	361.2	Phe1 to Asn3	1+	b_3 ion
506.9	507.2	Phe1 to Gln4	1+	y_4 ion

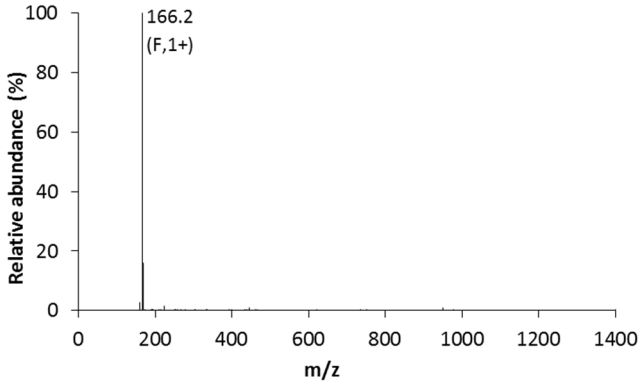

Figure S10: HPLC-ESI-MS spectrum of the terminal amino acid F, *Phe1*, with an elution time of 11.5 min. The singly charged (166.2) mass corresponding to *Phe1* is shown.

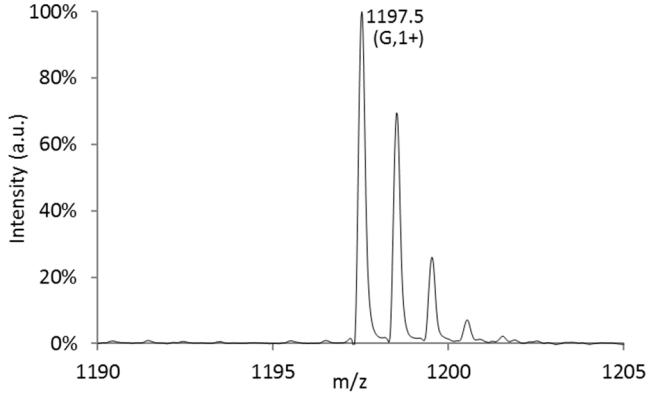

Figure S11: MALDI-TOF spectrum of singly charged peptide fragment G, *PyroGlu21 to Ala30* (1197.5) with its corresponding isotopic pattern.

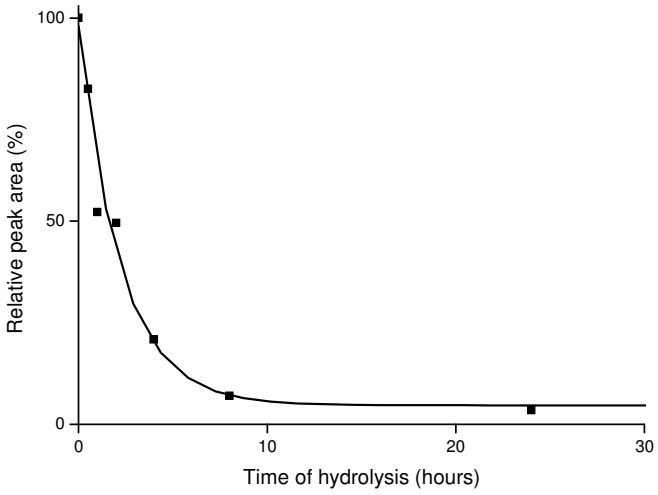

Figure S12: Kinetic plot showing the rate of disappearance of the parent peptide after incubation of oxidized insulin chain B with a Zr(IV) Wells-Dawson POM in a 2:1 molar ratio (Zr(IV) Wells-Dawson POM: oxidized insulin chain B) at 60 °C and pH 7.0.

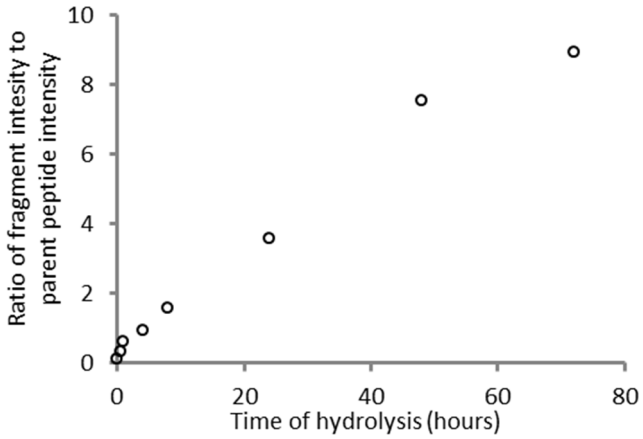

Figure S13: Ratio of intensity of peptide fragment, *Phe1----Gly8,* to intensity of oxidized insulin chain B over time at 37 °C and pH 7.0.

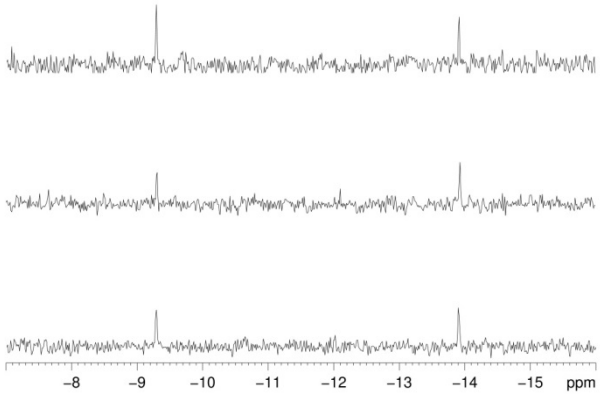

Figure S14: ^{31}P NMR spectra of Zr(IV) Wells-Dawson POM (0.5 mM, RT, pD 7.0) in the absence (bottom) and presence (middle) of oxidized insulin chain B (0.25 mM, RT, pD 7.0) and after heating the mixture (0.5 mM Zr(IV) Wells-Dawson POM + 0.25 mM oxidized insulin chain B, pD 7.0) at 60 ºC for 6 days (top) in D_2O.

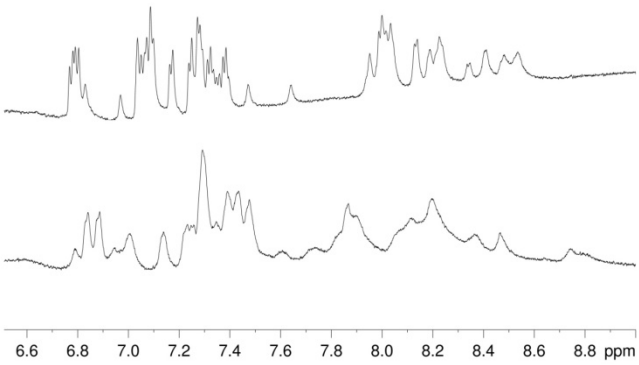

Figure S15: Aromatic and N-H region of ^{1}H NMR spectrum of oxidized insulin chain B in the absence (top) and presence (bottom) of Zr(IV) Wells-Dawson POM (pH 7.0, RT).

A. Sap, G. Absillis, T.N. Parac-Vogt, Dalton Transactions 44 (2015) p. 1539-1548
DOI: 10.1039/C4DT01477D

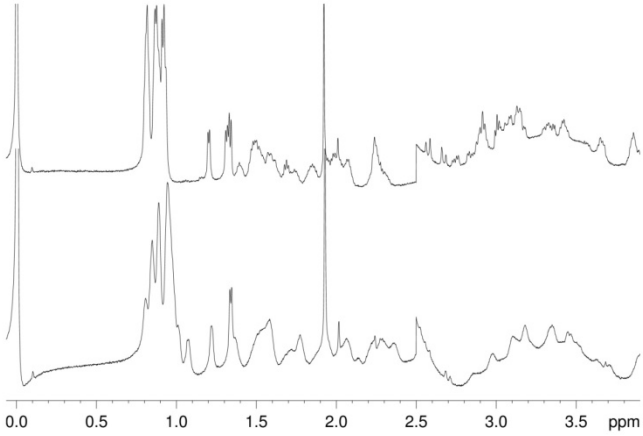

Figure S16: Aliphatic region of ^{1}H NMR spectrum of oxidized insulin chain B in the absence (top) and presence (bottom) of Zr(IV) Wells-Dawson POM (pH 7.0, RT).

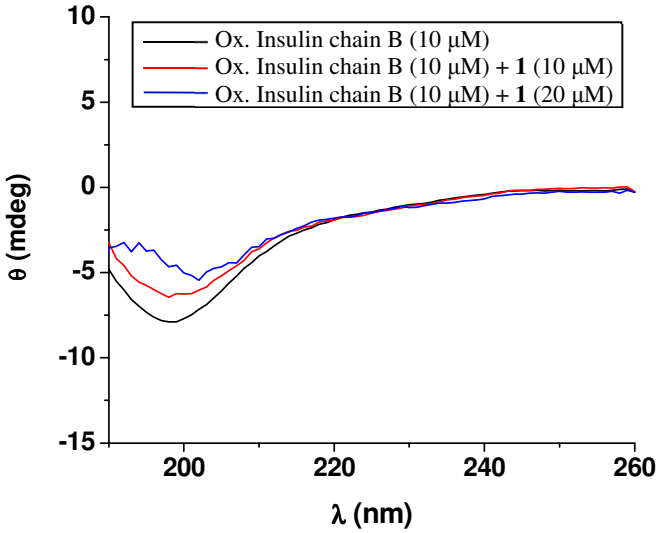

Figure S17: CD spectra of pure oxidized insulin chain B (10 µM) and oxidized insulin chain B (10 µM) in the presence of **1** (10 µM and 20 µM) in 100% H_2O (pH 7.0). A minimum at 200 nm is observed both in the absence and presence of Zr(IV) Wells-Dawson POM, representing a complete random coil conformation of oxidized insulin chain B.

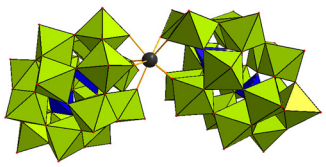

Figure S18: Combined polyhedral/ball-and-stick representation of $K_{13}(H_2O)[Eu(H_2O)_{3/4}(\alpha_2\text{-}P_2W_{17}O_{61})_2] \cdot 2\ KCl \cdot n\ H_2O$ **(2).** A 1:2 species is displayed in which one Eu (III) ion coordinates to two Wells-Dawson POM units. The WO_6 octahedrons are displayed in green, the PO_4 tetrahedrons in blue, and the Eu(III) ion center in dark grey.